Excited states in warm and hot dense matter

C. E. Starrett,* T. Q. Thelen, C. J. Fontes, and D. A. Rehn
Los Alamos National Laboratory, P.O. Box 1663, Los Alamos, New Mexico 87545, USA

(Received 22 September 2023; accepted 6 February 2024; published 4 March 2024)

Accurate modeling of warm and hot dense matter is challenging in part due to the multitude of excited states that must be considered. Here, we present a variational framework that models these excited states. In this framework an excited state is defined by a set of effective one-electron occupation factors, and the corresponding energy is defined by the effective one-body energy with an exchange and correlation term. The variational framework is applied to an atom-in-plasma model (a generalization of the so-called average atom model). Comparisons with a density functional theory based average atom model generally reveal good agreement in the calculated pressure, but our model also gives access to the excitation energies and charge state distributions.

DOI: 10.1103/PhysRevE.109.035201

I. INTRODUCTION

In warm and hot dense matter, the electronic structure comprises a complex and very large set of excited states of the Hamiltonian. Electrons are excited to populate these states through collisions and absorption of electrons and photons. The resulting properties of the plasma, such as the equation of state (EOS), opacity, and transport coefficients, can, in principle, be calculated by taking appropriate averages over these excited states. Experiments can probe these excited states in detail [1–7], providing stringent tests of our models.

There are many approaches to modeling warm and hot dense matter. Broadly speaking, at lower densities, a particularly successful approach is to start with the atomic structure of the isolated atoms or ions and then to correct for plasma effects [8–11]. The focus of such models is to calculate optical properties of the plasma, including absorption and emission spectra. Typically, these models become less successful at higher densities where a consistent treatment of plasma effects becomes crucial. At high densities, notable methods include path-integral Monte Carlo (PIMC) [12,13] and density functional theory (DFT) based simulations [14–19]. While the atomic methods focus on the properties of an atom or ion in the plasma, PIMC and DFT typically model many ions in a simulation cell and therefore contain a more sophisticated treatment of the plasma physics. PIMC has so far been largely limited to EOS applications and lower Z materials. The widely popular DFT [20], through its finite temperature extension [21], has been applied to a wide variety of properties and is generally very successful.

However, attempts to apply DFT to the opacity of moderately degenerate or nondegenerate systems reveal a weakness of the approach [22–24]. As shown in these references, the calculated opacities, using the independent particle method [25], differ dramatically from the measured data. These differences are most apparent in the bound-bound lines (see Fig. 3 of Ref. [22], for example). Whereas the atomic approaches agree relatively well with the data, the DFT based result is very different.[1] From a practical point of view, the important difference between the atomic and DFT approaches is the absence of so-called configurational broadening. This effect stems from variations in integer occupations of the electron states included in atomic approaches but not in DFT, which uses Fermi-Dirac occupation. These variations in occupation lead to different excited state energies and result in shifts (in energy) of the bound-bound lines. This is absent in the independent particle approach to opacity in DFT. Hence, one strong line centered at one transition energy in the spectra appears (see Fig. 3 of Ref. [22]), as opposed to many weaker lines in the atomic physics prediction. However, in DFT, it is the properties of the (thermal) equilibrium state of the system that are calculated. To calculate excited state properties, time-dependent (TD) DFT [25,26] or ensemble DFT (EDFT) [27–30] is required. In EDFT, another (nonthermal) ensemble is invoked to gain access to excited states, as discussed below.

TD-DFT calculations performed using the adiabatic local density approximation (ALDA) [31] fail similarly to the independent particle approach when applied to these opacity problems [24,32]. Although TD-DFT is exact in principle and allows for the calculation of all excited state properties, the ALDA uses only the instantaneous density for evaluation of the exchange-correlation functional. Multiple excitations are known to arise from nonadiabatic electron correlation effects that are neglected in the ALDA. This indicates that to properly treat multiple excitations, memory and dissipation effects need to be included explicitly in the exchange-correlation functional [33–36]. Hence, despite being exact in principle, in practice, for these plasma physics problems, the standard approximations (e.g., ALDA) are grossly inadequate.

The EDFT approach is an alternative to TD-DFT for calculating excited states and is perhaps more naturally suited for

*starrett@lanl.gov

[1]Notwithstanding the well documented exception of the quasicontinuum for the iron case.

inclusion of multiple excitations. This approach, formulated via a variational principle for ensembles of excited states, provides a modified Hohenberg-Kohn theorem that establishes an exact mapping between the potential and ensemble density. The benefit of this approach is that, via a corresponding Kohn-Sham scheme, the density for an ensemble of multiple excited states can be solved for simultaneously, and the energies of the excited states can be obtained. While this approach has that particular advantage, it is less frequently used than TD-DFT, and many open questions remain, such as how to construct exchange-correlation functionals that go beyond the "quasi-LDA" [37] and how to address the issue of ghost states [38], which are in some ways analogous to electron self-interaction in ground-state DFT. In addition, recent work has focused on a generalization of EDFT that allows for ensemble weights to vary independently [39] and, in principle, through a many-weight-dependent exchange-correlation functional, enables calculation of all excitation energies within a single simulation. Other recent work has focused on ways to decompose the correlation energy in EDFT into so-called state-driven and density-driven parts [40,41]. Note that temperature effects are not addressed in the EDFT approach. The approach we take in this paper is more similar to EDFT than to TD-DFT, although it is not formulated on a rigorous theoretical foundation and instead more closely follows atomic physics approaches for calculating excited states. However, unlike EDFT, temperature is included explicitly in our approach.

In DFT, the energy is that of a noninteracting system (that gives the same electron density as the full interacting system), which includes the exchange and correlation terms. Currently, the most accurate numerical scheme uses the Kohn-Sham (KS) approach [42]. In KS-DFT, the noninteracting energy is found by solving a single-particle Schrödinger equation for an effective one-body interaction potential, determined by minimizing the energy with respect to the density. This solution gives the eigenstates of this effective Hamiltonian, and the electronic density is constructed by filling these states according to Fermi-Dirac statistics. Even at elevated temperatures this scheme is used, resulting in a set of KS states that are fractionally occupied.

While these KS states are formally not physical states, their proximity to real, physical states is helpful for accurate predictions from the model and is reflected in, for example, the quantum shell structure observed in Hugoniot measurements [4,43,44]. At elevated temperatures, therefore, the KS scheme, in which variations in integer occupations of electron states are replaced by Fermi-Dirac occupations, is expected to be a poorer approximation than at zero temperature, where, in reality, there is only one occupied state (the ground state) [45].

A clue to a path forward may be found in the isolated atom approach to opacity [46,47]. In that field, an approach known as the configuration-average approximation is very similar in practice to the KS-DFT scheme. One constructs an effective one-body interaction potential for the ion or atom, includes an exchange and correlation correction, and solves the equations self-consistently. The key difference is that one does not use Fermi-Dirac occupations. Rather, one picks the occupations of the eigenstates to resemble desired excited states. Instead of there being one Fermi-Dirac occupied state, there are many different excited states, each corresponding to a particular distinct set of chosen occupations. This approach provides reasonable opacities in nondegenerate plasmas [2,46,47].

However, this isolated atom approach suffers from two major drawbacks when applied to the dense plasma regime: first, it generally ignores, or treats inconsistently, the free electrons; second, it is not variationally derived from an energy expression and so is generally not reliable for the EOS. A number of works have improved this situation [48–52], but a practical variational framework has remained elusive.

In this work, we give a variationally derived model that contains multiple distinct excited states and includes free electrons consistently. As in the isolated atom approach, the excited states are defined by a chosen set of occupations. The energy of each excited state is calculated from an effective one-particle system with exchange and correlation term. In the limit of one excited state with Fermi-Dirac occupations, this model recovers the Mermin-Kohn-Sham DFT. We give the derivation of this model and apply it to electronic structure and EOS calculations in the dense plasma regime. For the application considered (excited atoms in a plasma), the model can be viewed as an extension to the work of [53,54], where the author used DFT to get the averaged properties of an atom in a plasma.

The formal model is presented in Sec. II. We start with a general formalism for an arbitrary number of classical nuclei and a corresponding number of quantum mechanical electrons that make the system charge neutral. A free energy model is constructed, and in Secs. II B and II C, the constrained free energy is presented and minimized for this general system. In Sec. II D, we specialize to an atomic-like model with one nucleus in a sphere whose volume is given by the mass density and atomic mass. The model relies on the input of the choice of the excited state list, defined by a set of occupations. In Sec. II E, we show how the usual atomic-physics-like configuration definition can be practically extended into the positive energy continuum, thus including free states consistently. In Sec. III, we apply the atomic model to an example of an aluminum plasma to demonstrate its practicality and some of the features of the model.

II. FREE ENERGY

A. General model

We consider an ensemble of many classical nuclei and quantum mechanical electrons in a volume V at temperature T. In Hartree atomic units, the free energy of the system is

$$F = \sum_x W_x[E_x - TS_x] + T\sum_x W_x \ln W_x, \tag{1}$$

where the sum over x is over nondegenerate (in energy) electronic excited states (see the Appendix) and W_x is the probability of excited state x. The energy E_x is approximated by

$$E_x = E_x^{(0)} + E_x^{\mathrm{el}} + E_x^{\mathrm{xc}}, \tag{2}$$

where the effective single-particle kinetic energy is

$$E_x^{(0)} = \sum_{i\in x} n_{x,i} \int_V d^3r \psi_{x,i}^* \left(-\frac{1}{2}\nabla^2 \right) \psi_{x,i}, \tag{3}$$

with $\psi_{x,i}(\boldsymbol{r})$ being the orbital and $n_{x,i}$ being the occupation factor for the ith eigenstate, the set of which represents excited state x.[2] $E_x^{\rm el}$ is the electrostatic energy,

$$E_x^{\rm el} = \frac{1}{2}\int_V d^3r \int d^3r' \frac{n_x(\boldsymbol{r}) n_x(\boldsymbol{r}')}{|\boldsymbol{r}-\boldsymbol{r}'|} + \frac{1}{2}\sum_m \sum_{n\in V, n\neq m} \frac{Z_n Z_m}{|\boldsymbol{R}_n - \boldsymbol{R}_m|} - \sum_{n\in V} Z_n \int d^3r \frac{n_x(\boldsymbol{r})}{|\boldsymbol{r}-\boldsymbol{R}_n|}, \tag{4}$$

where $\boldsymbol{R}_i$ is the position vector of nucleus i, the sum over $n \in V$ is carried out over the nuclei in the volume V, $n_x(\boldsymbol{r})$ is the electron density of excited state x,

$$n_x(\boldsymbol{r}) = \sum_{i\in x} n_{x,i} |\psi_{x,i}(\boldsymbol{r})|^2, \tag{5}$$

and Z_n is the nuclear charge of nucleus n. $E_x^{\rm xc}$ is the exchange and correlation free energy, which we approximate with the local density approximation

$$E_x^{\rm xc} = \int_V d^3r\, \epsilon^{\rm xc}[n_x(\boldsymbol{r})]. \tag{6}$$

The entropy is split into two contributions (see the Appendix): a term due to the entropy of the excited state S_x,

$$S_x = -\int_V d^3r \sum_{i\in x} |\psi_{x,i}(r)|^2 \times [n_{x,i}\ln n_{x,i} + (1-n_{x,i})\ln(1-n_{x,i})], \tag{7}$$

and the term $\sum_x W_x \ln W_x$.

The essential idea here is that the excited states are approximated by a constrained one-particle system with one-particle eigenvectors $\psi_{x,i}(\boldsymbol{r})$ and occupations $n_{x,i}$. The thermal ensemble of excited states is then the set of these excited states with their probabilities $W_{x,i}$. The set of occupation factors $n_{x,i}$ is input into the model (see below).

B. Constrained free energy

Before minimizing this free energy, the following constraints are added:

$$\sum_{i\in x} \lambda_{x,i} \left[\int_V d^3r |\psi_{x,i}|^2 - 1 \right] = 0, \tag{8a}$$

$$B\left[\sum_x W_x - 1 \right] = 0, \tag{8b}$$

$$\gamma \sum_x W_x \left[\int_V d^3r n_x(\boldsymbol{r}) - Z_x \right] = 0, \tag{8c}$$

$$\sum_{x,i} \mu_{x,i} W_x \int_V d^3r |\psi_{x,i}(r)|^2 [n_{x,i} - f_{x,i}] = 0, \tag{8d}$$

where $\lambda_{x,i}$, B, γ and $\mu_{x,i}$ are Lagrange multipliers. Equation (8a) ensures normalization of the orbitals, Eq. (8b) ensures that the probabilities W_x sum to 1, Eq. (8c) requires overall charge neutrality of the excited states, and Eq. (8d) fixes the occupation factors $n_{x,i}$ to be given by the chosen inputs $f_{x,i}$. This last requirement is how we define an given excited state x. These can be chosen arbitrarily provided that $0 \leqslant f_{x,i} \leqslant 1$. In Sec. II E we will describe how they are chosen for a particular example.

C. Minimization of the free energy

We require the following to be true:

$$\frac{\delta\Omega}{\delta\psi_{x,i}^*(\boldsymbol{r})} = 0, \tag{9a}$$

$$\frac{\partial\Omega}{\partial n_{x,i}} = 0, \tag{9b}$$

$$\frac{\partial\Omega}{\partial W_x} = 0, \tag{9c}$$

where Ω is the constrained free energy. Applying the first of these, we obtain

$$0 = W_x \left\{ n_{x,i} \left[-\frac{1}{2}\nabla^2 + V_x^{\rm el}(r) + V_x^{\rm xc}(r) \right] - \lambda_{x,i} \right\} \psi_{x,i}(r) + W_x T [n_{x,i}\ln n_{x,i} + (1-n_{x,i})\ln(1-n_{x,i})]\psi_{x,i}(r) - W_x \gamma n_{x,i}\psi_{x,i}(r) - W_x \mu_{x,i} n_{x,i}\psi_{x,i}(r), \tag{10}$$

which can be rewritten as

$$\left[-\tfrac{1}{2}\nabla^2 + V_x^{\rm el}(\boldsymbol{r}) + V_x^{\rm xc}(\boldsymbol{r}) - \gamma \right] \psi_{x,i}(\boldsymbol{r}) = \epsilon_{x,i}\psi_{x,i}(\boldsymbol{r}), \tag{11}$$

i.e., the one-particle Schrödinger equation. γ is determined by setting the zero of the energy. Further,

$$V_x^{\rm el} = \frac{\delta E_x^{\rm el}}{\delta n_x(\boldsymbol{r})}, \tag{12}$$

$$V_x^{\rm xc} = \frac{\delta E_x^{\rm xc}}{\delta n_x(\boldsymbol{r})}. \tag{13}$$

The second minimization requirement, Eq. (9b), gives

$$0 = W_x \left[\int d^3r \psi_{x,i}^* \left(-\frac{1}{2}\nabla^2 \right) \psi_{x,i} + \int d^3r |\psi_{x,i}|^2 \left[V_x^{\rm el}(\boldsymbol{r}) + V_x^{\rm xc}(\boldsymbol{r}) - \gamma - \mu_{x,i} \right] \right] + T W_x \int d^3r |\psi_{x,i}|^2 \ln \frac{n_{x,i}}{1-n_{x,i}}, \tag{14}$$

which reduces to ($\beta = 1/T$)

$$n_{x,i} = \frac{1}{\exp[\beta(\epsilon_{x,i} - \mu_{x,i})] + 1}. \tag{15}$$

$\mu_{x,i}$ are then determined by the requirement that $n_{x,i} = f_{x,i}$, where $f_{x,i}$ is set by the input.

The third minimization requirement, Eq. (9c), gives

$$0 = F_x - B + T + T\ln W_x, \tag{16}$$

[2]Each excited state is approximated by an effective one-electron system with eigenstates $\psi_{x,i}(\boldsymbol{r})$ and occupations $n_{x,i}(\boldsymbol{r})$.

where $F_x = E_x - TS_x$; then

$$W_x = \frac{\exp(-\beta F_x)}{\mathcal{Z}}, \tag{17}$$

i.e., the usual Boltzmann factor, where

$$\mathcal{Z} = \sum_x \exp(-\beta F_x) \tag{18}$$

is the partition function.

This completes the model. First, one chooses a set of occupation factors that define the excited states $\{f_{x,i}\}$. Solving the one-particle Schrödinger equation (11) for the orbitals and eigenvalues associated with the xth excited state can then be carried out in the usual self-consistent field framework. The excited states are connected though the value of γ, which can be determined iteratively, although, as we shall see, the EOS does not seem to be sensitive to it for the cases tested here. Once the energies E_x and entropies S_x of the excited states are determined, the probabilities W_x are found with Eq. (17).

D. Application to the atomic model

In this section we specialize the formalism to the case of one atom in a sphere of volume V and radius R, where the volume is determined from the mass density and atomic mass, which are inputs to the model. Liberman [53] introduced the quantum average atom model. It is a DFT model of an atom in a charge neutral sphere. The model uses Kohn-Sham DFT with Fermi-Dirac occupation factors. Here, we extend this concept with the present excited state treatment. Due to the spherical symmetry of the atoms, the equations simplify somewhat. The kinetic energy can be written as

$$E_x^{(0)} = \sum_l 2(2l+1) \int d\epsilon\, n_{x,\epsilon,l} \int_0^R dr \times y^*_{x,\epsilon,l} \left(-\frac{1}{2}\frac{d^2}{dr^2} + \frac{l(l+1)}{r^2} \right) y_{x,\epsilon,l}, \tag{19}$$

where

$$\psi_{x,i}(\boldsymbol{r}) = \frac{y_{x,\epsilon,l}(r)}{r} Y_{l,m}(\hat{\boldsymbol{r}}), \tag{20}$$

$y_{x,l,\epsilon}(r)$ is the radial solution [55], l is the orbital angular momentum quantum number, and the eigenstate index i is replaced with ϵ and l. The entropy becomes

$$S_x = -\int_0^R dr \sum_l 2(2l+1) \int d\epsilon |y_{x,\epsilon,l}(r)|^2 \times [n_{x,\epsilon,l} \ln n_{x,\epsilon,l} + (1 - n_{x,\epsilon,l}) \ln(1 - n_{x,\epsilon,l})]. \tag{21}$$

The electrostatic energy is

$$E_x^{\rm el} = \frac{1}{2} \int_V d^3r \int_V d^3r' \frac{n_x(r) n_x(r')}{|\boldsymbol{r} - \boldsymbol{r}'|} - Z \int_V d^3r \frac{n_x(r)}{r}. \tag{22}$$

The exchange and correlation term is unchanged. The resulting Schrödinger equation is

$$\left[-\frac{1}{2}\frac{d^2}{dr^2} + \frac{l(l+1)}{r^2} + V_x^{\rm el}(r) + V_x^{\rm xc}(r) - \gamma \right] y_{x,\epsilon,l}(r) = \epsilon_{x,l} y_{x,l,\epsilon}(r). \tag{23}$$

We have brushed over an inconsistency inherent in average atom models, where the wave function is normalized over all space even though the energy involves only integrals inside the ion sphere. This issue has been much discussed in the average atom literature, and the same problem is inherent in the above atomic model and leads to a thermodynamically inconsistent model at low temperatures and high temperatures [56]. Note that the general model of Secs. II A, II B, and II C does not suffer from this inconsistency if, for example, we consider a periodic system. It is probably possible to derive a consistent atomic model, as was done for average atoms in Refs. [50,57], but we do not attempt that here. With this in mind, the pressure can be written as

$$P = -\left.\frac{\partial F}{\partial V}\right|_{T,N} = -\sum_x W_x \left[f_x(R) - \sum_{i\in x} \sum_l 2(2l+1) |y_{x,\epsilon,l}(R)|^2 \times n_{x,\epsilon,l}(\gamma + \mu_{x,\epsilon,l}) \right], \tag{24}$$

where $f_x(R)$ is the free energy density evaluated at R and

$$\gamma = \sum_x W_x V_x^{\rm xc}(R) \tag{25}$$

It is worth briefly contrasting the present atomic model with the superconfiguration model presented in Ref. [50]. While both present a variational model of configurations in plasmas, the model of Ref. [50] varies the sphere size depending on the excited state; the present model does not. Our model uses a configuration definition that is continuous across a pressure ionization, while it appears that in Ref. [50] the configuration does not exist if the bound state required by the configuration does not exist. Finally, the configuration model of Ref. [50] has not been amenable to practical implementation as yet, although an approximate version does exist [51].

E. Choosing the occupation factors

We now apply this atomic model to the calculation of the EOS in dense plasmas. The first step is to enumerate the states so that a list of all permutations can be created. There is an infinite set of possible excited states that one could consider based on variations of the occupation factors of bound and continuum electrons. With this in mind, we create an approximate, coarse enumeration of the states by defining energy boundaries $\epsilon_x^{n,l}$

$$2(2l+1) = \int_{\epsilon_x^{n,l}}^{\epsilon_x^{n+1,l}} d\epsilon\, \chi_{x,l}(\epsilon), \tag{26}$$

where $n = 1, 2, \ldots$. The first energy bound for a given l, $\epsilon_x^{1,l}$, is chosen to be just lower in energy than the lowest energy eigenstate for that l, and $\chi_{x,l}$ is the density of states for excited state x for angular momentum quantum number l,

$$\chi_{x,l}(\epsilon) = 2(2l+1) \int_V d^3r |y_{x,\epsilon,l}(r)|^2. \tag{27}$$

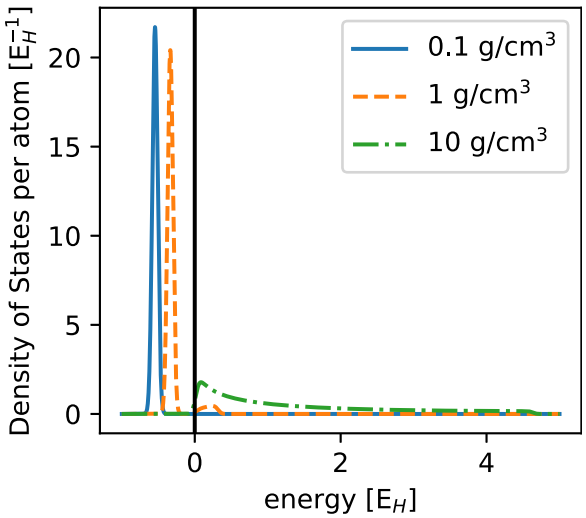

FIG. 1. Filled density of states for helium (units of hartrees, E_H). We have applied an arbitrary broadening of 1 eV to the DOS so that the bound states, which would otherwise be δ functions, can be displayed.

With the set of states defined by these energy ranges, we choose to occupy them with all perturbations of integer occupations, which is common in atomic physics approaches. We must also choose a maximum n to consider. The quantity n becomes equivalent to the principle quantum number for bound states that are well contained inside the ion sphere. Hence, for example, if we have a helium plasma and consider the maximum n to be 2 ($n_{\max} = 2$), we would have the following list of excited states: (1) $1s^2\,2s^0\,2p^0$, (2) $1s^1\,2s^1\,2p^0$, (3) $1s^1\,2s^0\,2p^1$, (4) $1s^0\,2s^2\,2p^0$, (5) $1s^0\,2s^1\,2p^1$, and (6) $1s^0\,2s^0\,2p^2$, and for configuration 2, for example, we have $n_{2,\epsilon_{1s},0} = 0.5$.

In Fig. 1 we show the filled DOS for configuration 1 in this example. At low densities the bound state is well contained within the ion sphere, and there are no free electrons. As density increases, the $1s$ orbital becomes partially bound, and two electrons cannot fit into the bound state, so the upper energy limit of this state extends into the continuum, satisfying the definition, Eq. (26). For the highest density, there are no bound states, and the $1s$ orbital extends into the continuum. We see that this atomic picture of excitations will be best if there are no (or very few) free electrons in the plasma since, in our example, for 10 g/cm^3, the two ionized electrons are spread evenly over the $1s$ band, which is only one possible distribution out of infinitely many.

There is another problem with this approach to occupation numbers just discussed—it will be prohibitively expensive for high temperatures or higher Z materials, for which $n_{\max}$ must be large. We solve this by treating all states with energies higher than $\epsilon_{x,\epsilon_x^{n_{\max}+1},l}$ with Fermi-Dirac statistics. The lifetime of excitations of core (deeply bound) states is relatively long, and that for excitations of continuum (free) electrons is much shorter due to collisions. Therefore, it is reasonable to create a set of occupation factors that include only a detailed list of excitations for the core states and use an average occupation [Fermi-Dirac (FD)] for the free electrons, at least for EOS purposes. In the results presented here we have used this approach. For our helium example, the list of excited states increases to include (7) $1s^1\,2s^0\,2p^0$ + FD, (8) $1s^0\,2s^1\,2p^0$ + FD, (9) $1s^0\,2s^0\,2p^1$ + FD, and (10) $1s^0\,2s^0\,2p^0$ + FD, where the occupation factors are Fermi-Dirac beyond the last energy boundary for each l runs, in principle, to ∞.

We note that by using Fermi-Dirac occupation factors in the definition of an excited state, the configurations become dependent on temperature, whereas in the first example, the electronic structure of the configurations and their energies are independent of temperature. For configurations that are independent of temperature, the resulting probabilities (populations) do depend on temperature but simply through the free energy ($F_x = E_x - TS_x$) and Eq. (17).

It is worth pointing out again that in this model, bound and free electrons are treated consistently. This is guaranteed by the fact that the definition, Eq. (26), gives smooth and continuous energy boundaries as a function of temperature and density, as well as the energy integral in Eqs. (19) and (21) being over all energies (i.e., over all bound and free eigenstates).

In summary, one starts with a list of configurations which define $n_{x,\epsilon,l}$. For an initial guess at γ and the potentials, one proceeds by solving Eq. (23) for the $y_{x,\epsilon,l}$ and eigenvalues for each of the configurations in the list. The electron density associated with each configuration is then constructed via Eqs. (5) and (20). Each configuration is then solved self-consistently, and the probabilities are updated via Eq. (17). γ is then updated [Eq. (25)], and the process is repeated until γ is self-consistent.

III. APPLICATION TO ALUMINUM PLASMAS

In Fig. 2, the charge state distribution (CSD) for aluminum plasmas is shown. Here, we calculate the charge of an ion by counting the number of positive energy electrons, which therefore includes electrons in resonance states. This is a reasonable definition, but we note that with this definition, it is possible to have an ion of noninteger charge. This can been seen from Fig. 1, where a bound state is partially bound for 1 g/cm^3. Physically, this behavior reflects the fact that as a bound state pressure ionizes, it is neither truly a bound nor a free electron state. In Fig. 2 we see that at the highest temperature (1000 eV) and lowest density (0.027 g/cm^3), the plasma is fully ionized. Going next to the 1000 eV, 2.7 g/cm^3 case, we find that the plasma is mostly fully ionized but contains about 20% of ions with a single bound electron. Increased collisional effects at this higher density are the cause of the lower average ionization.

For the 10 and 100 eV cases, we compare our results to the model of White *et al.* [58] (see Fig. 2). For the 100 eV, 2.7 g/cm^3 case our model is significantly more strongly peaked. For the 2.7 g/cm^3 cases we used $n_{\max} = 2$. In the limit of using $n_{\max} = 0$, we would recover the DFT result, and the CSD would be peaked at one charge state with all of the population. Using $n_{\max} = 1$ would allow some fluctuation, $n_{\max} = 2$ would allow even more, and so on. Hence, the reason the CSD of our model is more peaked than that of White *et al.* [58] is due to the lower value of $n_{\max}$. Does this mean that the result of the present model for this case is not converged with respect to $n_{\max}$? As we argued earlier, the present definition

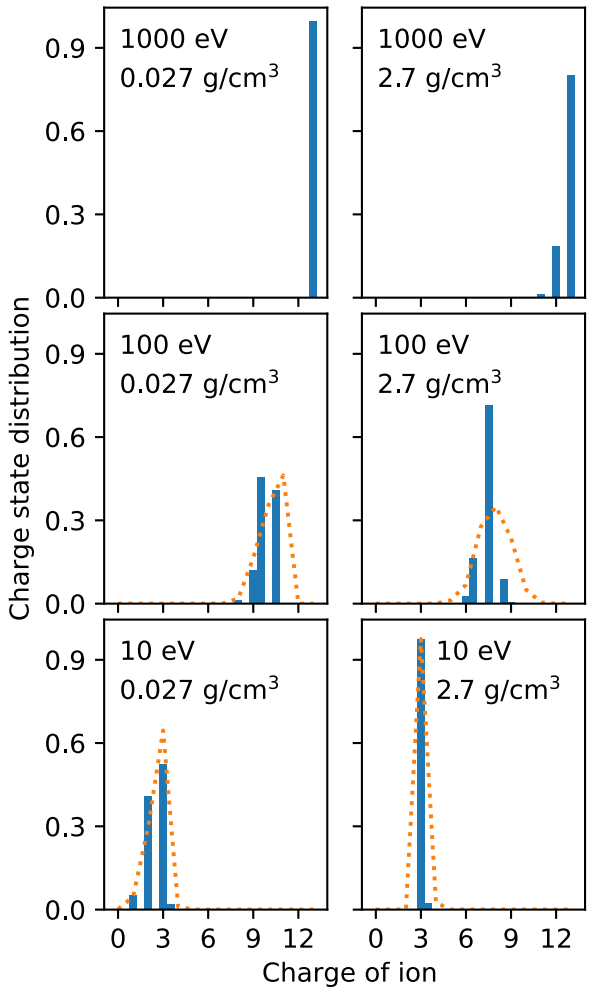

FIG. 2. Charge state distributions for aluminum plasmas. We have considered configuration perturbations up to the $n = 2$ shell for $2.7\,\mathrm{g/cm^3}$ and the $n = 3$ shell for $0.027\,\mathrm{g/cm^3}$. The results of the present model are shown by the blue bars. Also shown by the dotted lines are the results of Ref. [58].

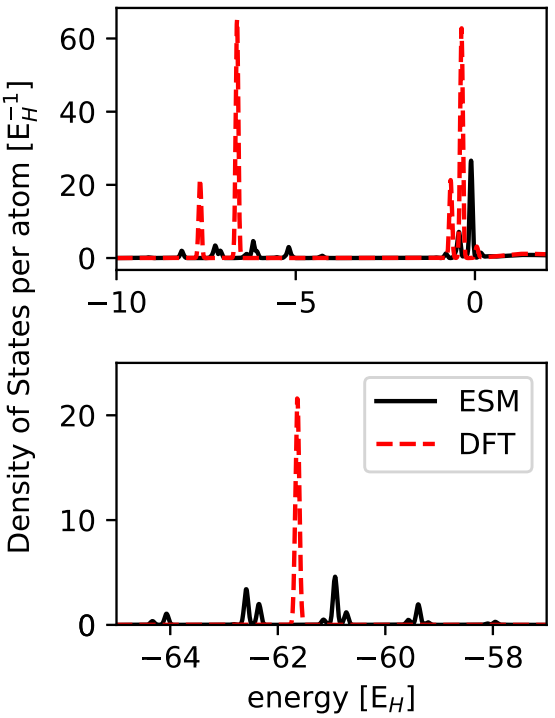

FIG. 3. Filled density of states for aluminum at 100 eV and $2.7\,\mathrm{g/cm^3}$. The solid black line is the result from the present excited state model (ESM). It is compared to the DFT prediction (dashed red line) from the average atom model TARTARUS [56].

of the excited state works best for core states. Using $n_{\max} = 2$ in this case ensures this outcome, while using $n_{\max} = 3$ would not, as the $n = 3$ states are partially bound. Which choice is more reasonable depends on the timescale of the experiment that we wish to model. Excitations of the partially bound $n = 3$ states will have a much shorter lifetime than those of the core states. For experiments that probe time-integrated quantities over timescales that are longer than the $n = 3$ excitation lifetimes, the present model is appropriate, whereas if the experiment has shorter time resolution, then considering explicit excitations of these shells would be necessary.

Last, we note that the CSD is an output of the model and we are free to choose different definitions of ion charge that are reasonable. This choice does not affect the model in any way—it does not change the EOS, energies, entropy, or populations.

In Fig. 3, the filled density of states is shown for a hot dense aluminum plasma at 100 eV and $2.7\,\mathrm{g/cm^3}$ using $n_{\max} = 2$. With aluminum's 13 electrons this leads to 63 distinct excited states, and the result shown is averaged over all of these with the probabilities W_x. In the bottom panel, we see the effect on the $1s$ eigenstate. There are four distinct groupings of $1s$ states. They correspond to four different charge states with significant probabilities in the plasma. In contrast, we also show the DFT result obtained using the TARTARUS code. There is only one peak, corresponding to the average $1s$ energy of the plasma. The different peaks within each cluster correspond to different arrangements of electrons in the "spectator" bound states (i.e., those in the $n = 2$ shell) but have the same ion charge.

In the top panel of Fig. 3, we again see a cluster of peaks from -10 to -5 hartrees (abbreviated E_H), corresponding to the $n = 2$ shell. The DFT results show two distinct peaks corresponding to the $2s$ and $2p$ eigenstates. Near zero energy, the line corresponding to the $n = 3$ states shows up. Since they are not explicitly included in our excited state list, the excited state model predicts a strong line near zero energy.

In Fig. 4, we show the radial density averaged over all excited states

$$n(\boldsymbol{r}) = \sum_x W_x n_x(\boldsymbol{r}). \tag{28}$$

We compare this to the DFT result from the TARTARUS model. Overall, we find good agreement, but some differences are observed. On the one hand, it is not surprising that the average over the excited states is not the same as the averaged excited state. On the other, the difference is fairly small and would be hard to test experimentally. Also shown in Fig. 4 are the electron densities from the excited states. These curves indicate that there is little fluctuation in the occupation of the

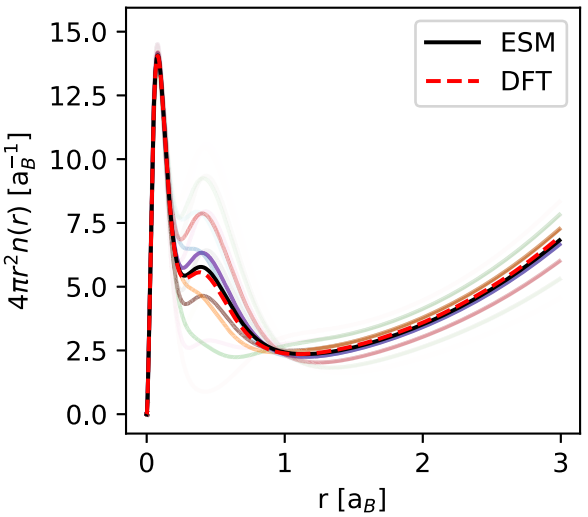

FIG. 4. Electron density of aluminum at 100 eV and 2.7 g/cm^3 (units of Bohr radii a_B). The solid black line is the predicted average radial density from the present excited state model (ESM). It is compared to the DFT prediction (dashed red line) from the average atom model TARTARUS [56]. Also shown by the semitransparent lines are the individual densities due to the excited states, with their degree of transparency proportional to the probability W_x.

1s shell (the peak nearest the origin), significant variation on the $n = 2$ shell occupation (the second peak from the origin), and significant variation in the free electron density (the tail after the peaks). We note that while the DOS (Fig. 3) indicates that the 1s eigenvalue does depend on the charge state, Fig. 4 shows that these variations do not strongly affect the density due to the 1s shell.

In Table I, the excess pressure is shown [given by Eq. (24), which does not include the ideal ion contribution] for the same aluminum plasmas, ranging from degenerate systems (2.7 g/cm^3 and 10 eV) to fully ionized (0.027 g/cm^3 and 1000 eV). These pressures are compared to TARTARUS results. Overall agreement is close between the two methods. Agreement is best for the high temperature cases, where details of the interaction potentials are unimportant due to the high average energy of the free electrons, as well as for the most degenerate case, where the plasma is dominated by one charge state (i.e., close to the DFT limit of the model). The remaining differences are relatively small and can be explained by the difference between calculating the pressure of an average system (DFT) versus the average pressure of the resolved excited states.

TABLE I. Values of excess pressure (in Mbar) for aluminum at temperatures of 10, 100, and 1000 eV and densities of 0.027 and 2.7 g/cm^3. ESM refers to the present excited state model, while TARTARUS refers to the DFT based average atom model [56].

	Al density = 0.027 g/cm^3	
	ESM ($n = 3$)	TARTARUS
10 eV	2.02×10^{-2}	2.16×10^{-2}
100 eV	0.954	0.948
1000 eV	12.5	12.5
	Al density = 2.7 g/cm^3	
	ESM ($n = 2$)	TARTARUS
10 eV	2.08	2.07
100 eV	64.4	65.4
1000 eV	1203	1201

The calculation of γ [Eq. (25)] requires an initial guess and an iterative, self-consistent procedure. We start with the value provided by an average atom model which seems to be close to the final answer. For example, for Al at 100 eV and 2.7 g/cm^3, the value from the TARTARUS model is $\gamma_{AA} = -0.446$ E$_H$ (which results in a pressure of 64.44 Mbar), while the converged value is $\gamma = -0.444$ E$_H$ (which results in a pressure of 64.41 Mbar). Conveniently, an approximation in which we choose γ to vary for each excited state such that $\gamma_x = V_x^{xc}(R)$ and using $\gamma = \sum_x W_x \gamma_x$ also seems to be accurate for EOS, giving $\gamma = -0.444$ E$_H$ and a pressure of 64.43 Mbar for this case. Clearly, this approximation could be more problematic for excitation energies (differences in excited state energies) than for the EOS, which is a more averaged quantity.

IV. CONCLUSIONS

A variational model of excited states in electronic structure was presented. The model recovers the usual Kohn-Sham density functional theory approach in the limit where only one state dominates (i.e., for degenerate systems like solids or for fully ionized plasmas). The model uses an effective one-electron expression for the excited state energy and includes the LDA for the exchange and correlation energy. Boltzmann factors for the excited state probabilities result from minimizing the free energy with respect to the probabilities.

Excited states are defined by a set of one-electron level occupation factors. If these are set to be the Fermi-Dirac occupation factors, then Kohn-Sham DFT is recovered. We applied this variational theory to a model of an atom in a plasma, a generalization of the average atom model [53,54]. We used an atomic physics-inspired definition of excited states, in which permutations of integer occupations of bound states are considered. A comparison of this application to the average atom model TARTARUS was made. We see the effect on the density of states, density, and pressure. In general, the pressure is quite close to the DFT calculation, but some differences were observed. Since DFT is a widely used and trusted method, this can be considered a validation of the current model. The advantage of the current approach is that the calculation of excited states should allow the prediction of more realistic optical properties with a consistent and realistic EOS. This advantage remains to be explored.

ACKNOWLEDGMENTS

LANL is operated by Triad National Security, LLC, for the National Nuclear Security Administration of the U.S. Department of Energy under Contract No. 89233218NCA000001.

APPENDIX: ENTROPY

The entropy is given by

$$S = -\sum_i W_i \ln W_i, \tag{A1}$$

where the sum is over all microstates of the system. If microstate i is degenerate, with g_x being the total number of microstates at the energy E_x, then

$$S = -\sum_x \sum_{i\in x} W_i \ln W_i. \tag{A2}$$

The probability of microstate i is $W_i = W_x/g_x$, so

$$\begin{aligned} S &= -\sum_x \sum_{i\in x} \frac{W_x}{g_x} \ln \frac{W_x}{g_x} \\ &= -\sum_x W_x \ln \frac{W_x}{g_x} \\ &= -\sum_x W_x \ln W_x + \sum_x W_x S_x. \end{aligned} \tag{A3}$$

[1] O. Ciricosta *et al.*, Direct measurements of the ionization potential depression in a dense plasma, Phys. Rev. Lett. **109**, 065002 (2012).

[2] T. Nagayama *et al.*, Systematic study of *L*-shell opacity at stellar interior temperatures, Phys. Rev. Lett. **122**, 235001 (2019).

[3] J. E. Bailey *et al.*, A higher-than-predicted measurement of iron opacity at solar interior temperatures, Nature (London) **517**, 56 (2015).

[4] A. L. Kritcher *et al.*, A measurement of the equation of state of carbon envelopes of white dwarfs, Nature (London) **584**, 51 (2020).

[5] L. B. Fletcher *et al.*, Ultrabright x-ray laser scattering for dynamic warm dense matter physics, Nat. Photon. **9**, 274 (2015).

[6] P. Hollebon, O. Ciricosta, M. P. Desjarlais, C. Cacho, C. Spindloe, E. Springate, I. C. E. Turcu, J. S. Wark, and S. M. Vinko, *Ab initio* simulations and measurements of the free-free opacity in aluminum, Phys. Rev. E **100**, 043207 (2019).

[7] S. M. Vinko *et al.*, Time-resolved XUV opacity measurements of warm dense aluminum, Phys. Rev. Lett. **124**, 225002 (2020).

[8] P. Hakel, M. E. Sherrill, S. Mazevet, J. Abdallah, Jr., J. Colgan, D. P. Kilcrease, N. H. Magee, C. J. Fontes, and H. L. Zhang, The new Los Alamos opacity code ATOMIC, J. Quant. Spectrosc. Radiat. Transfer **99**, 265 (2006).

[9] J. Colgan, D. P. Kilcrease, N. H. Magee, M. E. Sherrill, J. Abdallah, Jr., P. Hakel, C. J. Fontes, J. A. Guzik, and K. A. Mussack, A new generation of Los Alamos opacity tables, Astrophys. J. **817**, 116 (2016).

[10] C. A. Iglesias and F. J. Rogers, Updated OPAL opacities, Astrophys. J. **464**, 943 (1996).

[11] J. C. Stewart and K. D. Pyatt, Jr., Lowering of ionization potentials in plasmas, Astrophys. J. **144**, 1203 (1966).

[12] B. Militzer and K. P. Driver, Development of path integral Monte Carlo simulations with localized nodal surfaces for second-row elements, Phys. Rev. Lett. **115**, 176403 (2015).

[13] E. L. Pollock and D. M. Ceperley, Simulation of quantum many-body systems by path-integral methods, Phys. Rev. B **30**, 2555 (1984).

[14] L. Collins, I. Kwon, J. Kress, N. Troullier, and D. Lynch, Quantum molecular dynamics simulations of hot, dense hydrogen, Phys. Rev. E **52**, 6202 (1995).

[15] S. X. Hu, B. Militzer, V. N. Goncharov, and S. Skupsky, First-principles equation-of-state table of deuterium for inertial confinement fusion applications, Phys. Rev. B **84**, 224109 (2011).

[16] B. Holst, R. Redmer, and M. P. Desjarlais, Thermophysical properties of warm dense hydrogen using quantum molecular dynamics simulations, Phys. Rev. B **77**, 184201 (2008).

[17] C. E. Starrett and N. Shaffer, Multiple scattering theory for dense plasmas, Phys. Rev. E **102**, 043211 (2020).

[18] S. Zhang, H. Wang, W. Kang, P. Zhang, and X. T. He, Extended application of Kohn-Sham first-principles molecular dynamics method with plane wave approximation at high energy—from cold materials to hot dense plasmas, Phys. Plasmas **23**, 042707 (2016).

[19] B. Sadigh, D. Åberg, and J. Pask, Spectral-partitioned Kohn-Sham density functional theory, Phys. Rev. E **108**, 045204 (2023).

[20] P. Hohenberg and W. Kohn, Inhomogeneous electron gas, Phys. Rev. **136**, B864 (1964).

[21] N. D. Mermin, Thermal properties of the inhomogeneous electron gas, Phys. Rev. **137**, A1441 (1965).

[22] N. R. Shaffer and C. E. Starrett, Dense plasma opacity via the multiple-scattering method, Phys. Rev. E **105**, 015203 (2022).

[23] V. V. Karasiev, S. X. Hu, N. R. Shaffer, and G. Miloshevsky, First-principles study of *L*-shell iron and chromium opacity at stellar interior temperatures, Phys. Rev. E **106**, 065202 (2022).

[24] N. M. Gill, C. J. Fontes, and C. E. Starrett, Time-dependent density functional theory applied to average atom opacity, Phys. Rev. E **103**, 043206 (2021).

[25] A. Zangwill and P. Soven, Density-functional approach to local-field effects in finite systems: Photoabsorption in the rare gases, Phys. Rev. A **21**, 1561 (1980).

[26] E. Runge and E. K. U. Gross, Density-functional theory for time-dependent systems, Phys. Rev. Lett. **52**, 997 (1984).

[27] A. K. Theophilou, The energy density functional formalism for excited states, J. Phys. C **12**, 5419 (1979).

[28] E. K. U. Gross, L. N. Oliveira, and W. Kohn, Rayleigh-Ritz variational principle for ensembles of fractionally occupied states, Phys. Rev. A **37**, 2805 (1988).

[29] E. K. U. Gross, L. N. Oliveira, and W. Kohn, Density-functional theory for ensembles of fractionally occupied states. I. Basic formalism, Phys. Rev. A **37**, 2809 (1988).

[30] L. N. Oliveira, E. K. U. Gross, and W. Kohn, Density-functional theory for ensembles of fractionally occupied states. II. Application to the He atom, Phys. Rev. A **37**, 2821 (1988).

[31] C. A. Ullrich, *Time-Dependent Density-Functional Theory: Concepts and Applications* (Oxford University Press, Oxford, 2011).

[32] C. A. Ullrich, Time-dependent density-functional theory: Features and challenges, with a special view on matter under

extreme conditions, in *Frontiers and Challenges in Warm Dense Matter*, edited by F. Graziani, M. Desjarlais, R. Redmer, and S. Trickey (Springer, Cham, 2014), pp. 1–23.

[33] N. T. Maitra, F. Zhang, R. J. Cave, and K. Burke, Double excitations within time-dependent density functional theory linear response, J. Chem. Phys. **120**, 5932 (2004).

[34] C. A. Ullrich, Time-dependent density-functional theory beyond the adiabatic approximation: Insights from a two-electron model system, J. Chem. Phys. **125**, 234108 (2006).

[35] D. Sangalli, P. Romaniello, G. Onida, and A. Marini, Double excitations in correlated systems: A many–body approach, J. Chem. Phys. **134**, 034115 (2011).

[36] P. Elliott, S. Goldson, C. Canahui, and N. T. Maitra, Perspectives on double-excitations in TDDFT, Chem. Phys. **391**, 110 (2011).

[37] W. Kohn, Density-functional theory for excited states in a quasi-local-density approximation, Phys. Rev. A **34**, 737 (1986).

[38] N. I. Gidopoulos, P. G. Papaconstantinou, and E. K. U. Gross, Spurious interactions, and their correction, in the ensemble-Kohn-Sham scheme for excited states, Phys. Rev. Lett. **88**, 033003 (2002).

[39] K. Deur and E. Fromager, Ground and excited energy levels can be extracted exactly from a single ensemble density-functional theory calculation, J. Chem. Phys. **150**, 094106 (2019).

[40] T. Gould and S. Pittalis, Density-driven correlations in many-electron ensembles: Theory and application for excited states, Phys. Rev. Lett. **123**, 016401 (2019).

[41] E. Fromager, Individual correlations in ensemble density functional theory: State- and density-driven decompositions without additional Kohn-Sham systems, Phys. Rev. Lett. **124**, 243001 (2020).

[42] W. Kohn and L. J. Sham, Self-consistent equations including exchange and correlation effects, Phys. Rev. **140**, A1133 (1965).

[43] C. F. Ottoway, D. A. Rehn, D. Saumon, and C. E. Starrett, Effect of ionic disorder on the principal shock Hugoniot, Phys. Rev. E **104**, 055208 (2021).

[44] M. Bethkenhagen, A. Sharma, P. Suryanarayana, J. E. Pask, B. Sadigh, and S. Hamel, Properties of carbon up to 10 million kelvin from Kohn-Sham density functional theory molecular dynamics, Phys. Rev. E **107**, 015306 (2023).

[45] A. Gonis and M. Däne, Extension of the Kohn-Sham formulation of density functional theory to finite temperature, J. Phys. Chem. Solids **116**, 86 (2018).

[46] D. H. Sampson, H. L. Zhang, and C. J. F. Fontes, A fully relativistic approach for calculating atomic spectra for highly charged ions, Phys. Rep. **477**, 111 (2009).

[47] C. J. Fontes, H. L. Zhang, J. Abdallah, Jr., R. E. H. Clark, D. P. Kilcrease, J. Colgan, R. T. Cunningham, P. Hakel, N. H. Magee, and M. E. Sherrill, The Los Alamos suite of relativistic atomic physics codes, J. Phys. B **48**, 144014 (2015).

[48] N. M. Gill, C. J. Fontes, and C. E. Starrett, A superconfiguration calculation of opacity with consistent bound and continuum electron treatments using greens functions, J. Phys. B **56**, 015001 (2023).

[49] A. Bar-Shalom, J. Oreg, W. H. Goldstein, D. Shvarts, and A. Zigler, Super-transition-arrays: A model for the spectral analysis of hot, dense plasma, Phys. Rev. A **40**, 3183 (1989).

[50] T. Blenski and B. Cichocki, Variational approach to the average-atom-in-jellium and superconfigurations-in-jellium models with all electrons treated quantum-mechanically, High Energy Density Phys. **3**, 34 (2007).

[51] R. Piron and T. Blenski, Variational average-atom in quantum plasmas (VAAQP)–Application to radiative properties, High Energy Density Phys. **9**, 702 (2013).

[52] J.-C. Pain, F. Gilleron, Q. Porcherot, T. Blenski, and D. Benredjem, The hybrid detailed / statistical opacity code SCO-RCG: New developments and applications, AIP Conf. Proc. **1811**, 190010 (2017).

[53] D. A. Liberman, Self-consistent field model for condensed matter, Phys. Rev. B **20**, 4981 (1979).

[54] D. A. Liberman, INFERNO: A better model of atoms in dense plasmas, J. Quant. Spectrosc. Radiat. Transfer **27**, 335 (1982).

[55] T. Blenski and K. Ishikawa, Pressure ionization in the spherical ion-cell model of dense plasmas and a pressure formula in the relativistic Pauli approximation, Phys. Rev. E **51**, 4869 (1995).

[56] C. E. Starrett, N. M. Gill, T. Sjostrom, and C. W. Greeff, Wide ranging equation of state with tartarus: A hybrid Greens function/orbital based average atom code, Comput. Phys. Commun. **235**, 50 (2019).

[57] R. Piron and T. Blenski, Variational-average-atom-in-quantum-plasmas (VAAQP) code and virial theorem: Equation-of-state and Shock-Hugoniot calculations for warm dense Al, Fe, Cu, and Pb, Phys. Rev. E **83**, 026403 (2011).

[58] J. R. White, W. Johns, C. J. Fontes, N. M. Gill, N. R. Shaffer, and C. E. Starrett, Charge state distributions in dense plasmas, Phys. Plasmas **29**, 043301 (2022).